Draft version July 16, 2018
Typeset using LaTeX **twocolumn** style in AASTeX62

Disk Substructures at High Angular Resolution Program (DHARP): ?. Multiple ringed-structure in AS209

V. V. Guzmán et al.[1]

[1] *Joint ALMA Observatory*

ABSTRACT

All the emission can be explained by 7 concentric rings. The emission is axisymmetric. Gaps are not empty – CO emission is present within the gaps. We detect CO outside the millimeter dust edge (two outer rings?).

Keywords: circumstellar matter — planetary systems: formation, protoplanetary disks — dust

1. INTRODUCTION

Small intro on DHSARP program. In this paper we analyze the dust continuum and ^{12}CO $2-1$ emission in the disk around the AS 209 star. The 0.9 $M_\odot$ T Tauri star is a 1.6 Myr old and located 121± pc away (REFs).

2. OBSERVATIONS

Refer to overview paper Andrews et al. (2018) The AS 209 disk was observed with ALMA in Band 6 in September 2017 in configurations C40-8/9. Shorter-baselines were observed in May 2017 in configuration C40-5. We use additional archival data from projects 2013.1.00226 (Huang et al. 2016) and 2015.1.00486.S (Fedele et al. 2018), that provide information on shorter and intermediate baselines, respectively.

A detailed description of the data reduction process can be found in Andrews et al. (2018). Briefly, we first self-calibrated the short baselines, and in a second step self-calibrated the combined observations of short- and long-baselines. The improvement in the signal-to-noise was of a factor of X. The observations were cleaned in CASA 5.1, with multi-scale parameters.. and robust of 0. The resulting image has a beam of $X'' \times Y''$ and a r.m.s of X mJy.

The solutions of the self-calibration of the continuum emission where then applied to the ^{12}CO observations. The molecular line data was cleaned with a robust parameter of X, and a Keplerian mask was used to help the cleaning process. The resulting image has a beam of $X'' \times Y''$ and a r.m.s of X mJy.

3. RESULTS

3.1. *Dust continuum emission*

The dust continuum emission emission map is shown in the left panel of Fig. 1. The right panel shows the emission in polar coordinates. The emission is characterized by a series of concentric narrow rings. The inner disk encompasses rings located close together but resolved as distinct rings. The outer disk contains two rings that are well separated, and present similar brightness.

3.1.1. *Model-fitting in the uv-plane*

Given the striking ring-nature of the AS209 disk, we modeled the radial brightness distribution with the sum of concentric Gaussian rings:

$$I(r) = \sum_{i=0}^{N} A_i \exp(-(r - r_i)^2/2\sigma_i^2). \qquad (1)$$

The number of rings is chosen by a first eye-examination of the cleaned emission map and the deprojected radial profile (see Figs. 1 and 2). We include 4 rings in the inner (< 60 au) disk and 4 rings in the outer disk. The position of the innermost Gaussian is fixed to zero, i.e., the disk center. Two of outer rings correspond to the faint components near 100 and 140 au. We assume the emission is symmetric, and create synthetic visibilities given by the the Henkel transform (Pearson 1999):

$$V(\rho) = 2\pi \int_0^\infty I_\nu(r) J_0(2\pi\rho r) r dr \qquad (2)$$

where ρ is the deprojected uv-distance in units of $k\lambda$, r is the radial angular distance from the disk center in units of radians, and J_0 is the zeroth-order Bessel function of the first kind.

The observed visibilities are first deprojected, radially averaged and binned. We include uv-points from 10 to 10000 kλ, in steps of 10 kλ. To speed-up the fitting method, we only include visibilities $<$ 3000 kλ in the fit. The inclination (i), position angle (PA) and center of the disk, given by an offset (δ_x, δ_y), are included as free parameters in the fit. The total number of free parameters is then 27, that is 23 for the Gaussian rings (A_i, r_i, σ_i with i from 1 to 8) and 4 for the disk geometry (i, PA, δ_x, δ_y).

We use the `emcee` package (Foreman-Mackey et al. 2013), which is an implementation of the MCMC method, to sample the posterior distribution and find

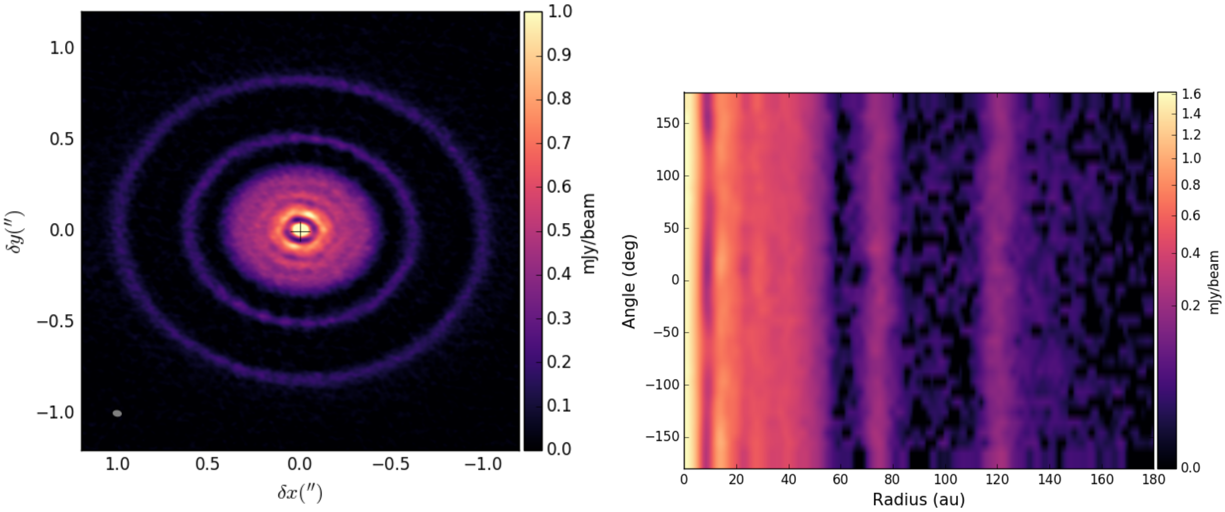

Figure 1. Dust continuum emission map (left), and in polar coordinates (right). The beam is shown in the bottom left.

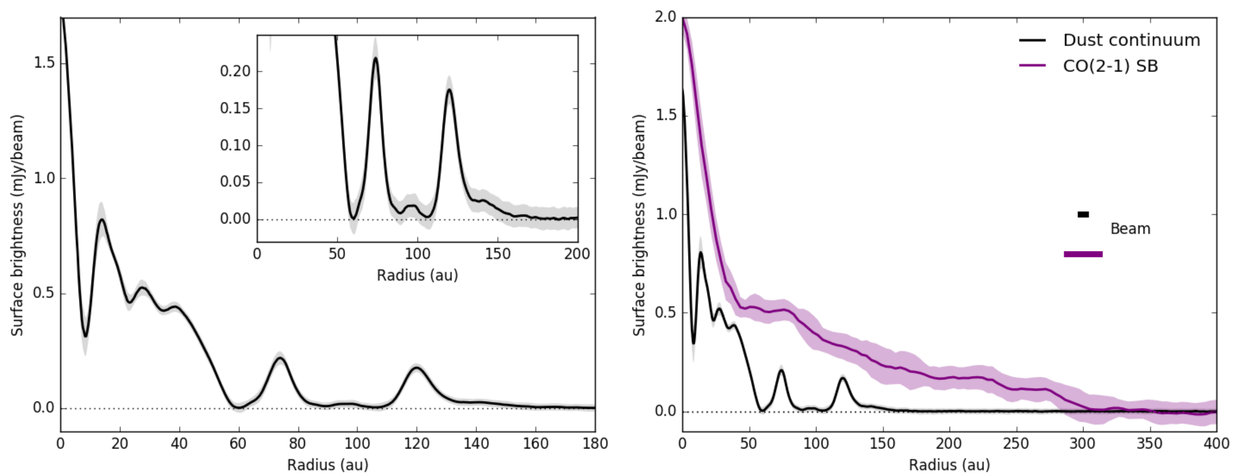

Figure 2. Deprojected radial profiles of the dust continuum emission (black lines). The ^{12}CO emission profile is shown in right panel (short-baselines only map).

the best-fit parameters. Table 1 summarizes the best-fit parameters. Fig. 4 shows the observed real part of the deprojected visibilities in black, using the best-fit disk inclination and position angle. The imaginary part of the visibilities are shown in light-blue (shifted by -30 mJy), and remain close to zero for all uv-distance, consistent with symmetric emission of the disk. A zoom of the $<$ 3000 kλ visibilities is shown in the upper-right panel of the figure. Our simple parametric model of pure Gaussian rings can recover most of the structure seen in the radially averaged visibility profile. The cleaned image of the best-fit model is shown in Fig. 5. The residuals, corresponding to the cleaned image of residual visibilities ($V_{obs} - V_{model}$) are shown in the right panel of the figure. Our best-fit model successfully reproduces the observations, as seen by the low-level emission in the residuals map. However, an asymmetry is seen in the inner disk, which suggests that the rings in the inner $\sim$ 10 au disk have a slightly different inclination than the rest of the disk. When the 2 faintest rings near 100 and 140 au are not considered, we find that the peak brightness of the rings decreases with distance, while the width of the rings increases with distance from the star. The 4 inner rings are narrower, with FWHM between 6 and 18 au, than the 2 outer bright rings which have FWHM of 23 and 25 au, respectively.

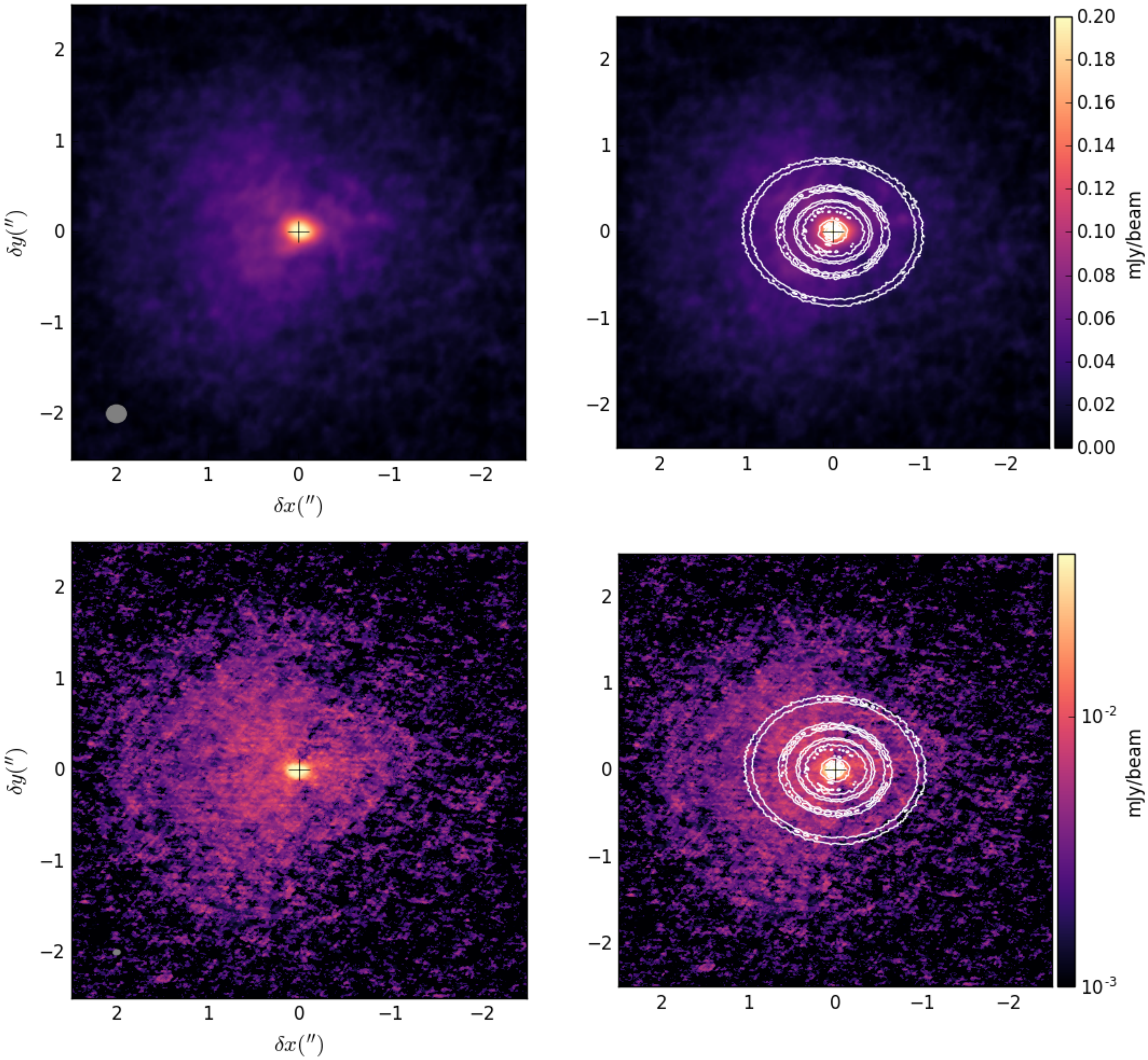

Figure 3. Moment-zero map of the ^{12}CO $2-1$ line. The maps shown in the upper panels include the short-baselines only. The lower panels include combined short+long baselines (beam is $0.075 \times 0.052''$). The dust continuum emission is shown in white contours in the right panels.

- Describe the surface brightness radial profile (the emission consists of a series of concentric narrow rings; the emission is axysimmetric; high contrast for the outer rings).

- Describe the fit done to the visibilities to extract the position and width of the ring components.

- Describe the main results: 1) All the emission can be explained by 7 concentric rings, 2) the rings are concentric, 3) a faint ring is found between the 2 outer rings, at around 100 au (the gap is not completely empty).

- Compare results with Jane's fit to the image.

3.2. *CO emission*

- Dust gaps are not empty. CO emission is present within the gaps.

- CO emission extends outside the millimeter dust edge. This shows the radial drift of large dust grains. Put limit on dust/co emission?

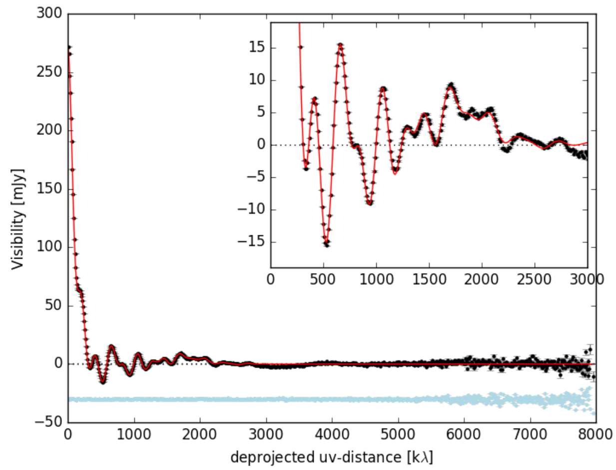

Figure 4. Observed (black) and modeled (red) deprojected visibilities. The imaginary part of the observed visibilities are shown in light-blue (shifted to -0.03 Jy). We only fit $u-v$ distances $< 3000k\lambda$, and assume the emission is axisymmetric.

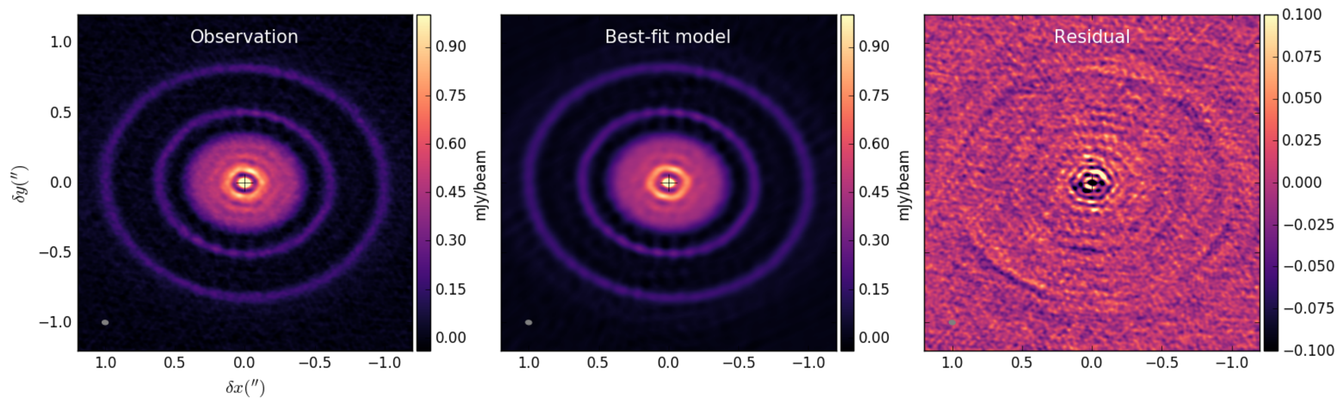

Figure 5. Observed dust emission map (left), the best-fit model (middle) and the residuals (right).

Table 1. Best-fit parameters.

Disk parameters		*Gaussian Rings parameters*								
i (deg)	34.9		Ring 1	Ring 2	Ring 3	Ring 4	Ring 5	Ring 6	Ring 7	Ring 8
PA (deg)	85.7	Rel. Amp	1.00	0.26	0.12	0.11	0.07	0.004	0.05	0.008
Offset-x (arcsec)	0.0017	R_c (au)	0.00	15.06	26.76	41.04	74.11	92.99	120.47	138.38
Offset-y (arcsec)	-0.0031	FWHM (au)	6.51	7.48	11.66	17.99	7.31	22.79	9.62	24.72

- There are 2 rings outside the millimeter dust emission. Need to confirm this. Maybe we want to show channel maps.
- Note the change of the slope at 50 au.

4. DISCUSSION

- Compare with rings in HL Tau and TWHya. The continuum emission in the AS209 disk shows deeper gaps.
- Discuss possible explanations for the formation of the gaps. Dust trapping (refer to Dullemond et al. 2018). The low viscosity model shown in Fedele's paper predict that a single planet can create multiple gaps in the disk, but this gaps are not completely empty. We do observe faint emission between the 2 main outer rings, which is consistent with these models.

- Compare ^{12}CO and dust. Huang et al (2016) detected C^{18}O extended emission that spatially coincides with the outer dust ring. With ^{12}CO we trace the disk surface.

5. SUMMARY

REFERENCES

Fedele, D., Tazzari, M., Booth, R., et al. 2018, A&A, 610, A24

Foreman-Mackey, D., Conley, A., Meierjurgen Farr, W., et al. 2013, Astrophysics Source Code Library, ascl:1303.002

Huang, J., Öberg, K. I., & Andrews, S. M. 2016, ApJL, 823, L18

Pearson, T. J. 1999, Synthesis Imaging in Radio Astronomy II, 180, 335